International Journal of Adhesion & Adhesives 118 (2022) 103249

Contents lists available at ScienceDirect

International Journal of Adhesion and Adhesives

journal homepage: www.elsevier.com/locate/ijadhadh

A detailed surface characterization study of SBA-15 and B-SBA-15-x mesoporous materials using the IGC technique

Tuğba Yarbaş [a], Alime Çıtak [b,*]

[a] Chemical Engineering Department, Bilecik Seyh Edebali University, 11100, Bilecik, Turkey
[b] Chemical Engineering Department, Eskişehir Osmangazi University, 26040, Eskişehir, Turkey

ARTICLE INFO

Keywords:
B-SBA-15
Mesoporous materials
Surface characterization
Adsorption thermodynamic parameters
Dispersive surface energy

ABSTRACT

Pure and boron-containing B-SBA-15-x (molar ratio, Si/B = 50, 30, 10) mesoporous materials were synthesized by a direct hydrothermal procedure. Samples were characterized by XRD, ICP-OES, FT-IR, BET and SEM. Inverse gas chromatography (IGC) technique was used to determine the dispersive surface energies (γ_S^d), adsorption thermodynamic parameters (ΔH, ΔG, ΔS) and the acid-base constants (K_A and K_D) of the samples. IGC experiments were performed at infinite dilution region at 200, 210, 220 and 230 °C. The surface characterization results confirmed that the SBA-15 structure was formed, boron was added to the structure and all samples have meso pores. The surface area of the pure SBA-15 was determined as 745.288 m^2/g and it was found that the surface area decreases with increasing boron content. Physical adsorption occurred between the IGC probe molecules and all SBA-15 materials according to the adsorption thermodynamic parameters. (γ_S^d) values of pure SBA-15, B-SBA-15-50, B-SBA-15-30 and B-SBA-15-10 were found at 40.873, 37.039, 36.636 and 37.444 mJ/m^2 at 200 °C, respectively. It has been observed that the dispersive surface energy of all samples decreases with increasing temperature. According to the S_C value calculated from the K_A and K_D parameters, the surface of B-SBA-15-10 with the highest boron content was found to be acidic. On the other hand the surfaces of all other samples were determined as basic.

1. Introduction

Mesoporous materials are preferred in many adsorption applications due to their high surface area and adjustable pore size. Usage areas of meso-porous materials are still being studied and their use as catalyst supports is becoming more common. Compared to other porous materials, SBA-15 is characterized by larger pores, thicker walls and higher thermal and hydrothermal stability [1–4].

Synthesis of SBA-15 with various active components enhancing surface activity is frequently encountered in the literature [5–9]. Transition metals and some acids are often used as active ingredients due to their activity in catalytic reactions. Boron is an important semi-metal due to its many uses in industry such as cosmetics, pharmaceuticals, adhesives, refractories, disinfectants, catalysts etc. In addition, there are results in the literature that boron doped catalysts show resistance to coke formation [10–12]. There are a few studies of SBA-15 with added boron in the literature [5,7]. Therefore, in this study, B-SBA-15-x samples were characterized by the IGC technique and both adsorption thermodynamic parameters and dispersive surface energy components of surface energy were calculated.

There are many approaches to preparing SBA-15 materials such as changing the active component and the synthesis method [4]. It is known that the final material structure is affected by the synthesis method used. Generally, direct hydrothermal and sol-gel methods are preferred in the synthesis of metal-loaded SBA-15 materials [5,7,10,13].

Surface free energy (SFE, γ_S) can be defined as the work required to produce a new material surface and is given by the relationship between surface area and energy [14]. γ_S includes dispersion and specific terms. The dispersive term (γ_S^d) is caused by non-polar interactions based on London forces and the specific term (γ_S^{sp}) is caused by polar interactions. Due to the high sensitivity of (γ_S^d) for changes in the surface chemistry, (γ_S^d) is an appropriate parameter for the characterization of porous materials [15]. It is known that determination of γ_S^d provides information about the force fields of high energy regions of adsorbent materials [16–18].

It is difficult to determine the surface energies of solids. Inverse gas

* Corresponding author.
E-mail address: acitak@ogu.edu.tr (A. Çıtak).

https://doi.org/10.1016/j.ijadhadh.2022.103249
Received 2 February 2022; Accepted 11 August 2022
Available online 17 August 2022

chromatography (IGC) is an important technique used for the surface characterization (superficial phenomena, glass transitions, dispersive surface energy, adsorption heat, acid-base properties) of solid materials [19]. Therewithal IGC is a reliable technique that provides accurate measurement regardless of sample morphology over a wide temperature range [20]. Contrary to conventional gas chromatography, in this method the non-volatile stationary phase in the column is examined. An empty column is filled with the porous material (adsorbent) under investigation and the probe molecule (adsorbate) in the mobile phase probes the surface of the adsorbent [21]. In summary, the IGC technique is based on determining the properties of solid materials using probe molecules of known properties. The retention times of the probe molecules on the solid are determined and γ_S^d is calculated.

In recent years, studies using IGC technique for the characterization of various materials have been carried out [15,19,21–24]. The dispersive surface energy of SBA-15 (surface area: 576 m^2/g) was found to be 56.03 mJ/m^2 at 366 K by using the IGC technique in one of these studies [15]. However, IGC characterization of boron-containing SBA-15 mesoporous materials has not been studied before.

In this study, pure and boron-containing SBA-15 samples were synthesized with the direct hydrothermal method. Samples were characterized by X-ray powder diffraction (XRD), Fouirer Transform Infrared Spektrofotometre (FTIR), N2 adsorption-desorption, Brunauer–Emmett–Teller (BET), İndüktif Eşleşmiş Plazma-Optik Emisyon Spektrometresi (ICP-OES) and scanning electron microscope (SEM) In order to understand the adsorption behaviors of synthesized materials, dispersive surface energies, adsorption thermodynamic parameters and acid-base constants (K_A and K_D) were determined by the IGC technique.

2. Experimental

2.1. Catalyst preparation

Pure SBA-15 was synthesized by a hydrothermal procedure [1,2]. Pluronic 123 triblock copolymer (Aldrich) and TEOS (tetraethyl orthosilicate) (Aldrich) were used as surfactant and silica source, respectively. 2.005 gr P123 was dissolved in 15 ml of water. 60.75 g of aqueous 2 M HCl was added to the solution under stirring. The solution was heated at 35 °C for 1 h. 4.27 g of tetraethylorthosilicate (TEOS) was added and the mixture was stirred at 35 °C for 20 h. The solution was then transferred to an autoclave and aged in a vacuum oven at 100 °C for 24 h. The solid product was recovered by filtration, washed and dried overnight. Calcination was conducted at 540 °C under a dry air flow for 6 h with a heating rate of 1°Cmin^{-1}.

B-SBA-15-x samples were also synthesized by direct hydrothermal procedure. In a synthesis procedure of B-SBA-15 samples [7], 4,02 g of Pluronic 123 was dissolved in 25 ml of water at 30 °C. 125 ml of aqueous HCl at required pH value was added to the solution under stirring. This was then heated at 40 °C for 1 h 8.6 g of tetraethylorthosilicate (TEOS) was added and the mixture was stirred at 40 °C overnight. A calculated amount of boric acid (molar ratio of Si/B = 50, 30, 10) was dissolved in water and added to the solution under stirring. The solution was then aged at 100 °C for 24 h under static conditions. The solid product was recovered by filtration and dried at 100 °C overnight. The template was removed by calcination under a dry air flow at 540 °C for 6 h with a heating rate of 1°Cmin^{-1}.

2.2. Characterization

Small angle XRD patterns were acquired on a Rigaku Ultima-IV X-Ray diffraction device operating at 40 kV and 30 mA using Cu Kα radiation (λ = 0.15406 nm). The diffractograms were recorded in the 2θ range of 0.5–10° with a 2θ step size of 0.01°.

Fourier-transform infrared spectra (FT-IR) patterns of samples were recorded on a Perkin Elmer Spectrum 100 spectrometer in the wavelength range of 400–4000 cm^{-1} and with a resolution of 0.4 cm^{-1} (ATR technique).

Chemical compositions of the B-SBA-15-x samples were measured using ICP-OES optical emission spectroscopy on a Anton Paar MW3000, Perkin Elmer Optima 4300DV spectrometer. Previously, samples were digested by acid treatment with HNO_3, HCl and HF.

Surface areas and N_2 adsorption–desorption isotherms of the samples were measured via N_2 adsorption at −196 °C on a Micromeritics ASAP 2020 apparatus with all samples outgassed at 250 °C for 180 min under vacuum before measurement.

Scanning electron microscopy (SEM) images were obtained with a JEOL JSM-5600 LV microscope (at 20 kV, x2000 zoom and 10 μm for all samples).

Inverse gas chromatography (IGC) experiments were performed with an Agilent 6890 GC, equipped with a thermal conductivity detector (TCD). A 4.66 mm i.d. and 50 cm length stainless steel column was used in this work. Helium was used as the carrier gas at a flow rate of 20 and 30 ml/min. The temperature of the injector and column was set at 200, 210, 220 and 230 °C to perform different experiments. 215.15 °C, which the standard average of 200, 210, 220 and 230 °C, was used in the calculation of adsorption thermodynamic parameters. The TCD detector was set at 300 °C for all experiments. Chromatographic peaks were recorded at the infinite dilution region. In this region, the retention volume was assumed to be independent of the injection amount [25]. Probes were injected manually with a 1 μl Hamilton syringe. The injection volumes were 0.01 (two times), 0.02 (three times) and 0.03 μl (two times) (at infinite dilution region). At least seven injections were made for each probe (previously averaged for each within itself, and then three results were averaged). Retention times were recorded with a chart recorder and corrected for the dead time of column. The average retention time value, t_R, was used for the calculations. To determine the adsorption themodynamic parameters and the surface energies of the solids *n-pentane, n-hexane, n-heptane* and *n-octane* were used. Three types of organic compounds with different acidity character were used as probe molecules in the calculation of acid-base parameters and SC values. *Dichloromethane (DCM)* and *trichloromethane (TCM)* were used as acidic probes, *tetrahydrofuran (THF)* was used as a basic probe and *diethylether (Et_2O)* and *acetone (Ace)* were used as amphoteric probes.

2.3. Theory and equations

2.3.1. Inverse gas chromatography theory

IGC experiments were conducted within the infinite dilution region (Henry's law region). The following formulas were used for calculations in this region (Eqs. (1) and (2)) [26–28].

$$V_N = (t_R - t_m).F_a.(T / T_a).j \tag{1}$$

$$j = \frac{3}{2}.\frac{\left[(P_{in}/P_{out})^2 - 1\right]}{\left[(P_{in}/P_{out})^3 - 1\right]} \tag{2}$$

Where V_N is the net retention volume of the probes, t_R is the probe retention time, t_m is the retention time of the mobile phase, F_a is the volumetric flow rate (at the column outlet), T is the column temperature, T_a is the ambient temperature, j is the James–Martin gas compressibility correction factor, P_{in} is the inlet pressure and P_{out} is the outlet pressure. (V_N) can be calculated according to Eq. (1) and Eq. (2) expresses the James–Martin gas compressibility correction factor.

At zero surface coverage, ΔH^0 can be identified by the differential heat of adsorption of the probe, which is based on the change of V_N with temperature (Eq. (3)).

$$\Delta H^0 = -R(d(lnV_N) / d(1 / T)) \tag{3}$$

(V_N) values are calculated according to eq (1). Then the lnV_N versus 1/T is plotted and ΔH^0 is calculated from the slope according to Eq. (3).

The standard free energy change of adsorption (ΔG^0) is calculated according to Eq. (4).

$$\Delta G^0 = -RTln\left(\frac{V_N.P_0}{m.S.\Pi_0}\right) \quad (4)$$

Where R is the ideal gas constant, P_0 is the adsorbate vapor pressure in the gaseous standard state equal to 101 kN/m^2 (101 kPa), m is the mass of adsorbent in the column, S is the specific surface area of adsorbent, and Π_0 is the reference two-dimensional surface pressure equal to 0.338 mN/m [23,29]. Since P_0, m, S and Π_0 are constant, the same equation can be written as (Eq. (5)):

$$\Delta G^0 = -RTlnV_N + C \quad (5)$$

The standard entropy change of adsorption (ΔS^0) can be calculated according to Eq. (6) [16,30–33].

$$\Delta S^0 = \left(\Delta H^0 - \Delta G^0\right) / T \quad (6)$$

2.3.2. Determination of dispersive surface enegy

The standard free energy change of adsorption (ΔG^0), work of adhesion (W_A) and surface energy of solid (γ_S), can be expressed as the sum of their own dispersive term (caused by non-polar interactions) and specific term (caused by polar interactions, OH groups), as an Eqs. (7)–(9) respectively.

$$\Delta G^0 = \Delta G^d + \Delta G^{sp} \quad (7)$$

$$W_A = W_A^d + W_A^{sp} \quad (8)$$

$$\gamma_S = \gamma_S^d + \gamma_S^{sp} \quad (9)$$

Where ΔG^d, ΔG^{sp}, W_A^d, W_A^{sp}, γ_S^d, γ_S^{sp} are dispersive and specific terms of ΔG^0, W_A and γ_S, respectively. γ_S^d values were calculated from the data obtained by using non-polar n-alkane series as probes. Similarly, γ_S^{sp} can be calculated from data obtained using polar probes (DCM, TCH, THF, Ace). The relationship between ΔG^0 and W_A is given by Eq. (10):

$$\Delta G^0 = N.a.\ W_A \quad (10)$$

Where N is the Avogadro constant and a is the cross-sectional area of the liquid molecule. The dispersive term of work of adhesion (W_A^d) is given by Eq. (11) [34]:

$$W_A^d = 2\sqrt{\gamma_S^d\ \gamma_L^d} \quad (11)$$

Where (γ_L^d) is the dispersive surface energy of liquid [35]. The relationship between (ΔG^0) and (V_N) is given in Eq. (5). By combining Eqs. (5), (10) and (11), the relation between γ_S^d and (V_N) can be obtained and the new equation can be expressed by Eq. (12) [26].

$$RTlnV_N = 2N\left(\gamma_S^d\right)^{1/2} a\left(\gamma_L^d\right)^{1/2} + const. \quad (12)$$

According to Eq. (12), γ_S^d values of samples were calculated from the slope of the line formed by plotting $a(\gamma_L^d)^{1/2}$ values against $RTlnV_N$ values, based on the retention volumes obtained using non-polar n-alkanes. The n-alkane line is obtained by using the $a(\gamma_L^d)^{1/2}$ and $RTlnV_N$ values for the n-alkanes. The $a(\gamma_L^d)^{1/2}$ and $RTlnV_N$ values of each of the polar probes are also marked separately on this graph. Mathematically, the distance of the point from the line is equal to ($-\Delta G^{sp}$) [26]. The ($-\Delta G^{sp}$) values were calculated but the graphs are not shown in this paper.

Eq. (13) shows the relationship between the specific component of Gibbs free energy change (ΔG^{sp}) and the specific component of enthalpy change ΔH^{sp}.

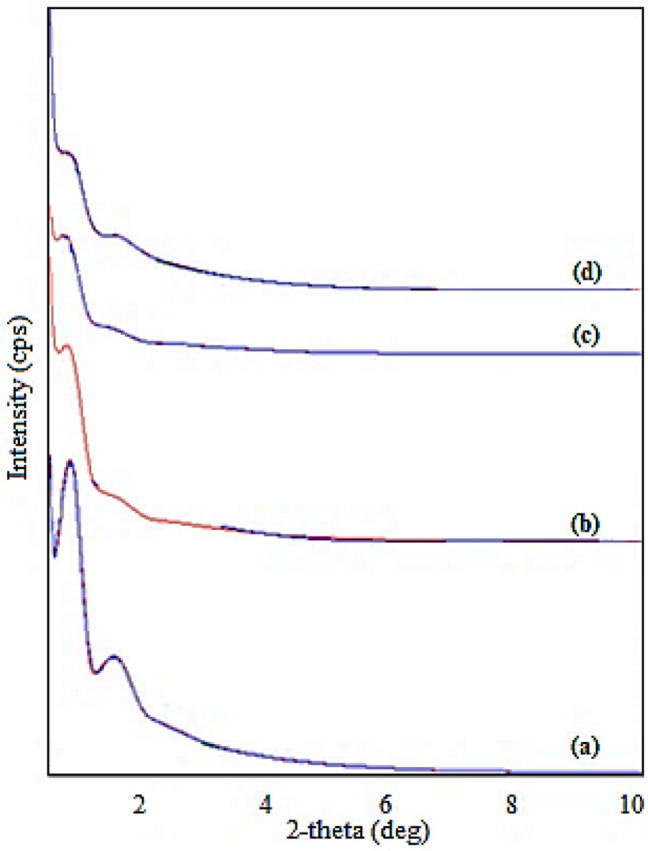

Fig. 1. Small angle XRD patterns (a) Pure SBA-15, (b) B-SBA-15-50, (c) B-SBA-15-30 and (d) B-SBA-15-10.

$$\Delta H^{sp} = -T^2.(\delta / \delta T)(\Delta G^{sp} / T) \quad (13)$$

For each polar component, when the values calculated according to Eq. (12) are plotted against temperature *(1000/T* versus *(− ΔG^{sp}/T))*, the ($-\Delta H^{sp}$) values can be calculated from the slope of the obtained line (Eq. (13)).

Eq. (14) can be used to find the acceptor and donor numbers (acid and base coefficients, K_A and K_D, respectively) of the solid surface [36].

$$\left(-\Delta H^{sp} / AN^*\right) = K_A.(DN / AN^*) + K_D \quad (14)$$

Where DN and AN^* are Gutmann's donor and modified acceptor numbers, respectively [22,37,38].

(S_C) is a measure of the surface acidity and basicity, which is calculated from the ratio of (K_D/K_A) (Eq. (15)).

$$S_C = |K_D / K_A| \quad (15)$$

According to Eq. (15), for a (S_C) > 1, the surface is considered to be alkaline, but acidic for (S_C) < 1 [23].

3. Results and discussion

3.1. XRD analyses

Small angle XRD patterns of all samples are shown in Fig. 1. The intensity values for each sample are between 0 and 300000 cps. When the data of all samples are shown in the same graph, they overlap and the lines cannot be separated. Therefore, for clarity, the combined graph was added, ignoring the intensity values.

SBA-15 and B-SBA-15-x samples all showed a sharp peak (approximately at 2θ = 0.88°) and two diffraction peaks (approximately at 2θ =

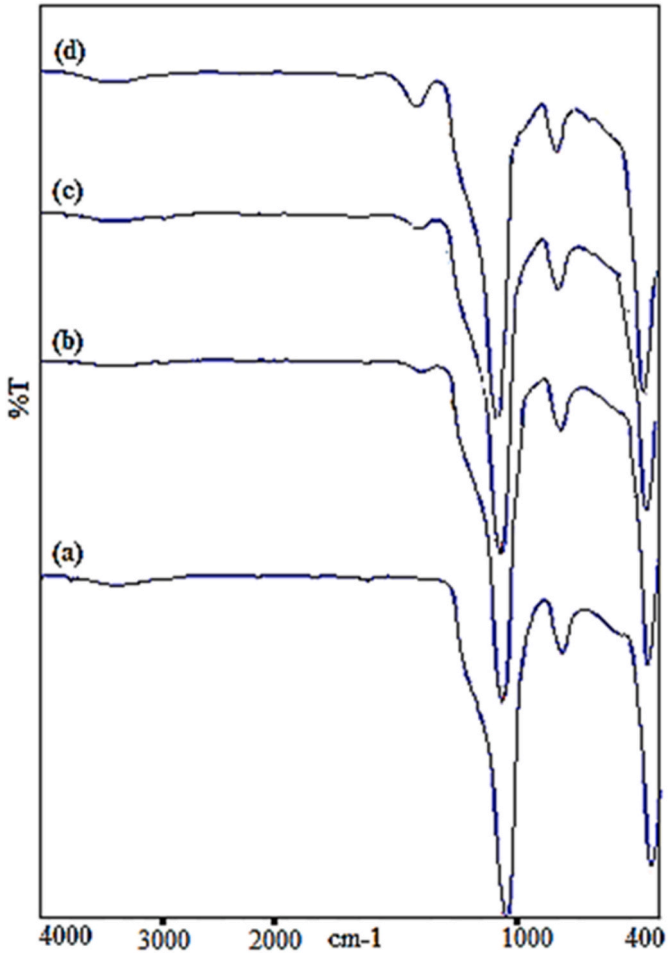

Fig. 2. Framework FT-IR spectra of (a) Pure SBA-15, (b) B-SBA-15-50, (c) B-SBA-15-30 and (d) B-SBA-15-10 catalysts.

1.5° and 1.88°) and these peaks represent (100), (110) and (200) reflections, respectively with typical attributes of two dimensional, well-arranged hexagonally mesoporous structure (p6mm symmetry) illustrating the high quality of mesopore packing [1,2,12]. XRD results proved that the SBA-15 structure is succesfully formed in all samples and the addition of boron to the structure did not change the basic structure of SBA-15. Also the results are compatible with the literature [5,7].

3.2. FT-IR measurements

FT-IR spectra of SBA-15 and B-SBA-15-x catalysts are shown in Fig. 2. According to the literature, the small shoulder band seen at 920 cm^{-1} in B-SBA-15-10, the sample with the highest boron content, is tetra coordinated boron in the framework [5,39]. The same peak was not seen in other boron containing samples. This may occur because the amount of boron loaded into other samples is too small. Also, by looking at previous studies with boron-containing materials, the 1395 cm^{-1} band seen only in B-SBA-15-x samples can be interpreted as the presence of boron species [5,12,40,41]. These adsorption bands show that boron oxide species were successfully formed on the surface of B-SBA-15-x samples. The bands at 429-441 cm-1 and 805-813 cm-1 in all samples can be interpreted as asymmetric and symmetric stretching vibrations of Si–O and the band at 1043-1059 cm-1 is thought to be the Si–O–Si band in all samples [6,10,12]. The pure SBA-15 shows a vibration at a wavelength of 1625 cm-1 which wasn't seen in other samples, that can be considered as adsorbed water. The band 3390-3442 cm-1 for all samples (not marked in the graph) indicates the presence of surface silanol groups and adsorbed water [6].

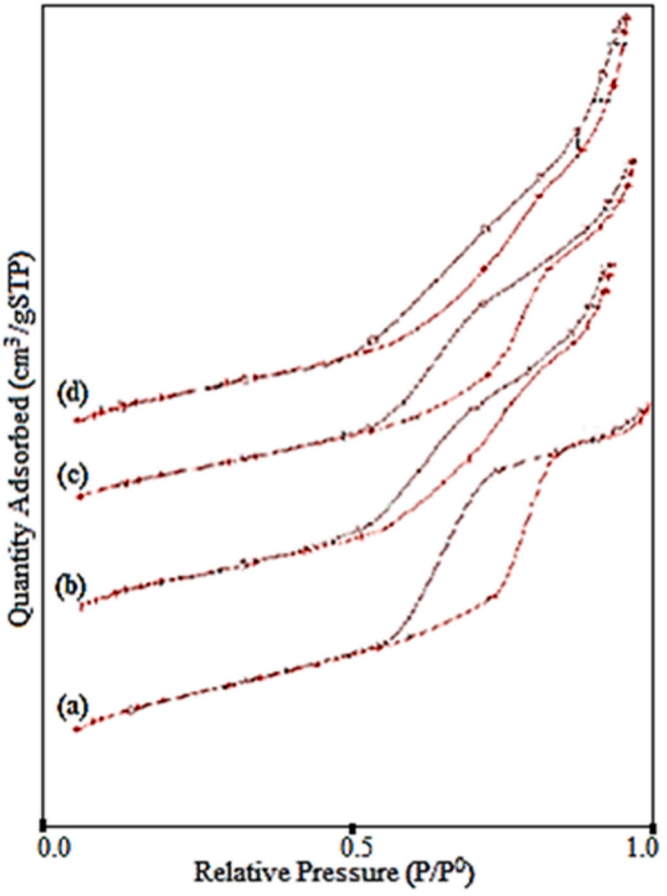

Fig. 3. N_2 adsorption isotherms of (a) Pure SBA-15, (b) B-SBA-15-50, (c) B-SBA-15-30 and (d) B-SBA-15-10 catalysts.

Table 1
ICP-OES results, BET surface areas, pore diameter and pore volumes of samples.

Sample	B content (wt%)[a]	A_{BET} (m^2/g)[b]	d_p (nm)[c]	V_p (cm^3/g)[d]
Pure SBA-15	0.000	745.288	6.56	1.06
B-SBA-15-50	0.294 ± 0.004	645.522	7.65	1.14
B-SBA-15-30	0.430 ± 0.010	644.184	7.91	1.17
B-SBA-15-10	1.050 ± 0.010	611.895	8.73	1.26

[a] ICP-OES results.
[b] BET Surface area.
[c] BJH Adsorption average pore width.
[d] BJH Adsorption cumulative volume of pores between 17.000 Å and 3000.000 Å width.

3.3. Determination of surface area and boron content studies

Textural properties such as N_2 adsorption-desorption isotherms, boron content by weight (ICP-OES), BET surface areas, average pore diameters and pore volumes were investigated for all samples. Results are given in Fig. 3 and Table 1, respectively. The quantity adsorbed values for each sample are between 140 and 840 cm^3/g STP. When the data of all samples are shown in the same graph, they overlap and the lines cannot be separated. Therefore, for clarity, the combined graph was added, ignoring the quantity adsorbed values.

It can be seen that all isotherms in Fig. 3 correspond to type IV of the IUPAC classification, representing mesoporous materials. All samples exhibited a clear H1-type hysteresis loop associated with a highly ordered mesoporous structure with narrow pore size distribution of cylindrical channels at high relative pressure values ($P/P^0 = 0.53–0.83$), which is consistent with results in the literature [5,7,10,12,42].

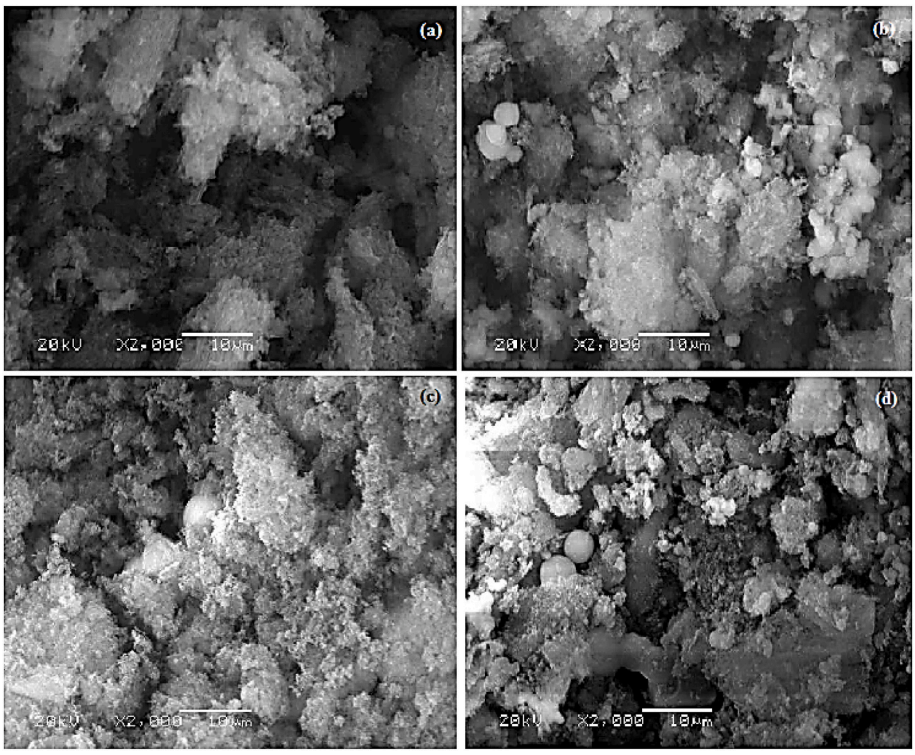

Fig. 4. SEM images of samples (for x2000 zoom). (a) Pure SBA-15, (b) B-SBA-15-50, (c) B-SBA-15-30 and (d) B-SBA-15-10.

According to Fig. 3, pure SBA-15 showed the isotherm most similar to type IV. The isotherms of the B-SBA-15-x samples also confirm to type IV, but they showed narrower hysteresis rings compared to pure SBA-15. This may be due to boron added to the structure at different amounts. As explained above, the quantity adsorbed values were approximately found to be within the same range for all samples (140–840 cm^3/g STP). However, it is seen in Table 1 that the boron contents, BET surface areas, pore diameters and pore volumes of the samples are different.

According to the ICP-OES results (Table 1), the boron contents by weight of the samples were found as %1.05 (B-SBA-15-10), 0.43 (B-SBA-15-30), 0.29 (B-SBA-15-50) and 0 (pure SBA-15), respectively. This result is expected because the synthesis calculations were made according to the n_{Si}/n_B molar ratio. Therefore, B-SBA-15-10 with the lowest n_{Si}/n_B ratio has the highest boron content.

Pure SBA-15 exhibits 745.288 m2/g surface area which is in agreement with the literature [10,12,43]. The surface area ranking is as follows: pure SBA-15 > B-SBA-15-50 > B-SBA-15-30 > SBA-15-10 (745.288, 645.522, 644.184 and 611.895 m2/g, respectively). It is reasonable that increasing amount of boron added to the structure may cause the reducing surface area. And this may occur because the boron atoms added to the structure partially block the pores. In the literature, there are SBA-15 samples prepared with ratios SiO2/B2O3 = 50 and 10 and their surface areas were found to be 767 and 672 m2/g, respectively [5]. However, in our study, the samples were prepared with molar ratios nSi/nB = 50, 30 and 10. Therefore, the composition by weight and surface areas of the materials are not similar compared with Eswaramoorthi and Dalai's study.

Pore size values of samples were found ranging between 6.56 and 8.73 nm. The pore size (6.56 nm) of pure SBA-15 is compatible with the 6.5 nm, 6.91 nm and 7.1 nm values found in the literature [10,12,15]. The pore sizes of the B-SBA-15-x samples are over 7.65 and there is a study in the literature where the pore diameter of a B-SBA-15 sample is 7.8 nm [5]. Therefore, it can be said that the results are compatible with the literature. It is seen that the pore size increases as the amount of boron in the structure increases. Generally, when an additional material is added to the structure, the pore size decreases as the amount of added material increases, and this is explained by the fact that new atoms partially block the pores [12,44]. However in Grieken's study, the pore diameters of the Al and Cr added SBA-15 samples were found to be higher than pure SBA-15, and this was explained by the lower wall thicknesses of the Al and Cr bonded structures [7].

It is observed that the pore volume increases with increasing boron content of the sample, as does the pore size. And the order is B-SBA-15-10 > B-SBA-15-30 > B-SBA-15-50 > Pure SBA-15 (1.26, 1.17, 1.14 and 1.06 cm3/g, respectively). There are studies in the literature where the pore volumes of pure SBA-15 are 0.93 [43], 0.96 [7], 0.98 [6], 1.19 [5] and 1.35 cm3/g [11]. These values are compatible with the 1.06 cm3/g value in our study. In addition, it is seen that the increase in boron content causes an increase in average pore diameter (d_p) and total pore volume (V_p). In Grieken's study, similar increasing trends were observed for Al, Cr-containing SBA-15 samples and B-containing SBA-15 samples synthesized by the hydrothermal method [7]. As a result of adding different components to the structure, the increase in average pore diameter and total pore volume is explained by inclusion of the added component into the silica walls [45].

The pore volume values of the B-SBA-15-x samples ranged from 1.14 to 1.26 cm3/g. In two different studies in the literature, the pore volumes of the boron added SBA-15 samples synthesized by hydrothermal methods were found between 0.99 and 1.14 cm3/g [5] and between 0.97 and 1.1 cm3/g [7], which is consistent with our results.

3.4. Scanning electron microscopy study

Fig. 4 shows SEM images where a rope-like structure is seen in all samples. Previous work has shown that rope-like structures are characteristic features of SBA-15 [1,2]. It is also observed that agglomerations tended to form with increasing boron content as shown in Fig. 4b, c, and d, respectively. A similar situation has been observed in a study in which SBA-15 with various boron contents was investigated [5].

Table 2
Physical and chemical properties of the probes.

Probes	a[a] (Å)^2	(γ_L^d)[a] (mJ/m^2)		DN[b] (kJ/mol)	AN*[b] (kJ/mol)	*Character*
n-Pentane	45.00	16.10	–	–	Neutral	
n-Hexane	51.50	18.40	–	–	Neutral	
n-Heptane	57.00	20.30	–	–	Neutral	
n-Octane	63.00	21.30	–	–	Neutral	
DCM	38.00	26.50	0.00	16.32	Acidic	
TCM	44.00	25.90	0.00	22.59	Acidic	
Et_2O	47.00	16.70	80.30	5.90	Amphoteric	
Ace	42.50	16.50	71.40	10.46	Amphoteric	
THF	45.00	22.50	84.42	2.09	Basic	

[a] [16,26,46].
[b] [46].

3.5. IGC measurements

Thermodynamic properties of probes are shown in Table 2. Graphs of $RTln(V_N)$ versus $a.(\gamma_L^d)^{1/2}$ for the adsorption of n-alkanes on the samples are shown in Fig. 5.

Table 3 shows the calculated dispersive surface energy values of the samples where it can be seen that the dispersive surface energy decreased with increasing temperature in all samples. In studies conducted with different materials in the literature, it has been understood that γ_S^d decreases with an increase in temperature [16,47]. Similarly, there are studies in the literature in which it is stated that γ_S^d depends on the surface composition of the solid and the test temperature [48,49]. The γ_S^d of pure SBA-15 was found to be 40.873 mJ/m^2 at 200 °C. In the literature, γ_S^d of pure SBA-15 determined by the IGC method was found to be 56 mJ/m^2 at 93 °C [15,22]. In addition, when approaching the zero surface coverage of different silica samples at 90 °C, it is seen that γ_S^d values change between approximately 30-50 mJ/m^2 using the IGC technique [24].

Graphs of $RTln(V_N)$ versus $a.(\gamma_L^d)^{(1/2)}$ for all samples were found to be linear at all temperatures (Fig. 5). And the γ_S^d values were determined from the slopes of the lines. In the literature, it has been suggested that γ_S^d can be obtained by extrapolation for different temperatures when the variation of γ_S^d as a function of temperature is linear [16]. According to this suggestion, when extrapolated using our operating temperatures of 200 and 210 °C, which are closest to 93 °C, and γ_S^d values at these temperatures, the γ_S^d value of pure SBA-15 is calculated as 59.18 mJ/m^2 at 93 °C. This value is compatible with the literature (56 mJ/m^2 [15,22].

No γ_S^d results for SBA-15 containing boron has been found in the literature to compare with our B-SBA-15-x values. In fact, γ_S^d values of the samples containing boron were found very close to each other at all temperatures. This may occur because even B-SBA-15-10 with the highest boron content contains a very small amount of boron by weight (1 wt%, Table 1).

γ_S^d order of the samples varies according to the temperatures. However, the only unchanged sequence is that the γ_S^d of pure SBA-15 is highest at all temperatures and the γ_S^d of B-SBA-15-30 is the lowest. In the literature, there are studies in which the addition of some components to the surface of materials (not SBA-15) reduce the γ_S^d and surface free energy [48–51]. Accordingly, it is interpreted that the γ_S^d values of

Table 3
Calculated dispersive surface energy values of samples for different temperatures.

	γ_S^d (mJ/m^2)			
Sample	**200°C**	**210°C**	**220°C**	**230°C**
Pure SBA-15	40.873	39.167	35.712	32.036
B-SBA-15-50	37.039	33.394	29.757	27.015
B-SBA-15-30	36.636	31.316	28.148	24.900
B-SBA-15-10	37.444	33.779	28.679	26.842

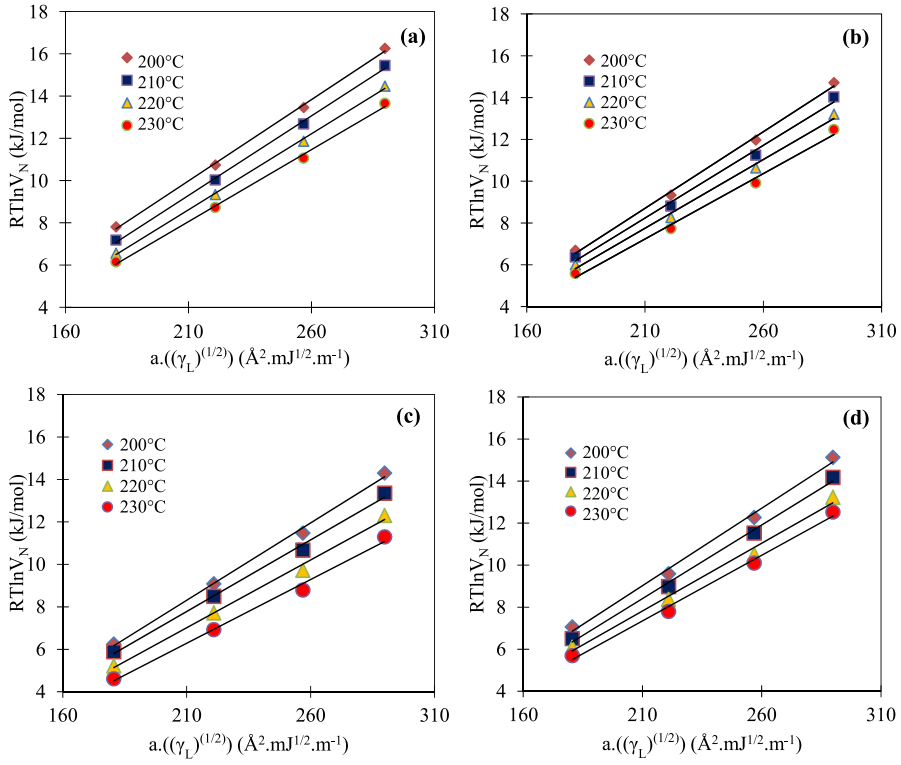

Fig. 5. RTln(V_N) versus a.$(\gamma_L^d)^{1/2}$ plots for the adsorption of n-alkanes on samples for different temperatures. Pure SBA-15, (b) B-SBA-15-50, (c) B-SBA-15-30 and (d) B-SBA-15-10.

Table 4
Thermodynamic parameters for the adsorption of the probes on pure SBA-15 and B-SBA-15-x samples.

Sample	Probes	-ΔH (kJ/mol)	-ΔG (kJ/mol)	-ΔS (kJ/molK)
Pure SBA-15	n-Pentane	38.357	5.674	0.066
	n-Hexane	46.612	8.457	0.078
	n-Heptane	55.354	11.020	0.090
	n-Octane	61.905	13.716	0.098
	DCM	36.505	5.283	0.064
	TCM	41.553	7.456	0.069
	Et_2O	64.227	14.565	0.101
	Ace	59.196	14.413	0.091
	THF	67.264	16.892	0.103
B-SBA-15-50	n-Pentane	28.296	5.491	0.046
	n-Hexane	38.825	7.867	0.063
	n-Heptane	48.141	10.278	0.077
	n-Octane	54.574	12.948	0.085
	DCM	26.063	4.908	0.043
	TCM	30.532	6.677	0.048
	Et_2O	56.094	12.690	0.088
	Ace	44.171	12.951	0.063
	THF	55.478	4.884	0.103
B-SBA-15-30	n-Pentane	36.706	4.830	0.065
	n-Hexane	47.477	7.402	0.082
	n-Heptane	58.081	9.518	0.099
	n-Octane	66.053	12.171	0.110
	DCM	36.409	4.208	0.065
	TCM	41.378	6.210	0.072
	Et_2O	66.118	12.417	0.110
	Ace	65.363	13.269	0.106
	THF	72.869	15.364	0.117
B-SBA-15-10	n-Pentane	32.459	5.887	0.054
	n-Hexane	41.977	8.239	0.069
	n-Heptane	51.880	10.658	0.084
	n-Octane	60.641	13.328	0.096
	DCM	29.217	5.247	0.049
	TCM	38.911	7.148	0.065
	Et_2O	59.883	12.853	0.096
	Ace	59.205	13.475	0.093
	THF	70.238	16.029	0.111

B-SBA-15-x samples are lower than that of pure SBA-15 at all temperatures, due to the fact that the boron addition affects the surface coverage.

The adsorption thermodynamic parameters (ΔH, ΔG and ΔS) of the samples calculated using Eqs. (3)–(6) are shown in Table 4. Adsorption equilibrium depends on changes in adsorption enthalpy and entropy. The Gibbs free energy change indicates the spontaneity of adsorption. Negative *(ΔG)* indicates that adsorption of adsorbate occurs spontaneously [52]. According to Table 4 the negative *(ΔG)* values of all probes for all samples indicated that the adsorption was spontaneous and the probe preferred to stay in the stationary phase rather than the mobile phase [53]. Generally, physical adsorption occurs when *(ΔG)* is between 0 and -20 kJ/mol, and chemical adsorption when it is between −80 and −400 kJ/mol [53,54]. It can be seen that all *(ΔG)* values are in the range of 0 to −20 kJ/mol. Therefore, all adsorbate-adsorbent interactions were interpreted as physisorption. Which bonds are formed in physical adsorption (hydrogen bonding, electrostatic, hydrophobic or van der Waals interactions) can be determined from thermodynamic parameters. According to the literature, all interactions given in Table 4 were caused by van der Waals interactions *($\Delta H<0$, $\Delta S<0$, $|\Delta H| > |T\Delta S|$)* [53].

A negative *(ΔH)* means that the adsorption of adsorbate is an exothermic process. Therefore, the negative value of the enthalpy change actually indicates that the process is energetically stable [55]. Physical adsorption occurs when *(ΔH)* < 40 kJ/mol [52,54]. Since all *(ΔH)* values in Table 4 are highly negative, it can be said that all adsorption processes were managed by physisorption control. According to the literature, the more negative adsorption enthalpy change (ΔH) indicates a higher interaction between the adsorbate and the adsorbent [16,25]. So it means that the interaction of pure SBA-15 with all probes

Table 5
($-\Delta G^{sp}$) values of polar probes on samples.

Sample	Probes	$-\Delta G^{sp}$ (kJ/mol)			
		200 °C	210 °C	220 °C	230 °C
Pure SBA-15	DCM	1.59	1.32	1.30	1.36
	TCM	1.41	1.40	1.22	1.14
	Et_2O	8.56	8.29	7.94	7.64
	Ace	9.76	9.55	9.23	8.96
	THF	9.26	8.96	8.83	8.42
B-SBA-15-50	DCM	1.62	1.50	1.15	1.41
	TCM	1.79	1.74	1.33	1.43
	Et_2O	7.19	6.61	6.43	6.04
	Ace	8.51	8.13	7.99	7.96
	THF	7.78	7.37	7.09	7.13
B-SBA-15-30	DCM	1.60	1.58	1.47	1.44
	TCM	1.57	1.46	1.33	1.22
	Et_2O	7.48	7.04	6.74	6.27
	Ace	9.74	9.15	8.77	8.40
	THF	9.07	8.47	8.23	7.88
B-SBA-15-10	DCM	1.66	1.42	1.54	1.24
	TCM	1.57	1.49	1.55	1.33
	Et_2O	6.90	6.59	6.08	5.83
	Ace	8.82	8.71	7.92	7.67
	THF	8.73	8.23	7.93	7.38

is higher than B-SBA-15-50. However, the same inference cannot be made for B-SBA-15-30 and B-SBA-15-10. (ΔH) values obtained on B-SBA-15-30 for n-hexane, n-heptane, n-octane, DEE, Ace and THF are more negative than pure SBA-15. In other words, it appears that B-SBA-15-30 interacts more highly with these probes. Similarly, the (ΔH) value obtained on B-SBA-15-10 for THF is also more negative than pure SBA-15. Negative values of (ΔH) indicate that free diffusion of molecules through a bulk solution and a boundary layer is less than that resulting from bulky groups and other adsorbate arrangements on the surface and pores of adsorbents [55].

All of the (ΔS) values are negative in Table 4. The negative entropy change corresponds to a decrease in the degrees of freedom of the adsorbed species [53,55]. In brief, the negative entropy change indicates that the system is more ordered after adsorbate adsorption [52].

In all samples, ($-\Delta H$), ($-\Delta G$) and ($-\Delta S$) values for n-alkanes increase as the C number increases. Considering the negativity, it can be seen that an increase in the C number appears to decrease ΔH, ΔG and ΔS (e.g. $-0.098 < -0.066$, ΔS values for n-octane and n-pentane on pure SBA-15, respectively). Almost the same situation was observed with the C number in other organic probes.

Another generalization that can be made by looking at Table 4 is that the ($-\Delta H$), ($-\Delta G$) and ($-\Delta S$) values obtained on pure SBA-15 using the same probes are mostly higher than those obtained in B-SBA-15-50 and B-SBA-15-10 samples (accept ($-\Delta G$) of n-pentane; ($-\Delta H$) and ($-\Delta S$) of Ace and THF on B-SBA-15-10).

The ($-\Delta G^{sp}$) values were calculated from the distance of the plotted points from the line according to the $RTlnV_N$ and $a(\gamma_L^d)^{1/2}$ values of the polar probes and are given in Table 5. According to Table 5, it can be said that increasing temperature decreases the ($-\Delta G^{sp}$) values for almost all samples and all probes (except for DCM on pure SBA-15 at 230 °C, TCM on B-SBA-15-50 at 230 °C, THF on B-SBA-15-50 at 230 °C and TCM on B-SBA-15-10 at 220 °C). It can be said that the interactions of all samples with polar probes are close to each other (Table 4). Therefore, it is estimated that the polar surface hydroxyl group densities of the samples are close to each other with small differences. However, pure SBA-15 appears to have the strongest interaction with amphoteric (Et_2O and Ace) and basic (THF) probes.

No study was found in the literature to calculate the ($-\Delta G^{sp}$) values using SBA-15 with boron content. However, a study was found in which pure SBA-15 was used and ($-\Delta G^{sp}$) values were calculated for some polar probes by the IGC method. (ΔG^{sp}) values for TCM (chloroform) and acetone on pure SBA-15 were found as −2.0 and −13.6 kJ/mol at the

Table 6
Acid-base parameters and surface character (SC) of pure SBA-15 and B-SBA-15-x samples.

Sample	K_A	K_D	S_C
Pure SBA-15	0.250	0.377	1.508
B-SBA-15-50	0.211	0.506	2.398
B-SBA-15-30	0.310	0.398	1.284
B-SBA-15-10	0.337	0.207	0.614

experimental temperature of 93 °C, respectively [22]. In our study, the $(-\Delta G^{sp})$ values of the same probes on pure SBA-15 at 200 °C (which is our operating temperature closest to 93 °C) were found as 1.41 (TCM) and 9.76 (Ace) kJ/mol (Table 5). As explained above, considering the proposition that a temperature increase, decreases the values of $(-\Delta G^{sp})$, it can be said that the results are compatible with each other.

Table 6 shows acid-base parameters (K_A and K_D) and surface character (S_C) of samples. The (K_A) ranking was found as: B-SBA-15-10 > B-SBA-15-30 > Pure SBA-15 > B-SBA-15-50. It can be seen that the acid parameter (K_A) increases with increasing boron content, except for B-SBA-15-50. The (K_D) ordering is more complex and is as follows: B-SBA-15-50 > B-SBA-15-30 > Pure SBA-15 > B-SBA-15-10. And finally, the (S_C) ranking is seen as B-SBA-15-50 > Pure SBA-15 > B-SBA-15-30 > B-SBA-15-10 which is exactly the opposite of the (K_A) ranking. According to this order, it cannot be said that increasing amounts of boron added to the structure affect the surface acidity proportionately.

It can interpreted that B-SBA-15-50 has the highest potential for specific interactions ($K_A + K_D$) (Table 6). Compared to the pure SBA-15, the K_D value of B-SBA-15-10 was significantly decreased due to the addition of a high amount of boric acid which changed the character of the sample. Because its S_C value is less than 1, B-SBA-15-10 has an acidic surface. Except for B-SBA-15-10, the surface characters of all samples were found to be alkaline. B-SBA-15-50 has the highest basicity among the alkaline samples.

K_A and K_D values of pure SBA-15 were found as 0.25 and 0.377, respectively. Since the K_D value is higher than K_A, the surface character was found to be basic. In Rückriem's study, K_A and K_D values of pure SBA-15 were found to be 0.7 and 0.52, so it can be said that the surface is acidic [22]. It is thought that this discrepancy may arise from differences in the pure SBA-15 synthesis steps in the two studies.

4. Conclusions

Inverse gas chromatography (IGC) at infinite dilution is a suitable method for determining the dispersive surface energy and adsorption thermodynamic parameters of SBA-15 mesoporous materials. It was determined that all adsorption processes were physical adsorption. In all samples, (-ΔH), (-ΔG) and (-ΔS) values for n-alkanes increased as the C number increased. According to $(-\Delta H)$ values, the most interacting materials with probe molecules were determined as pure SBA-15 and B-SBA-15-30 mesoporous materials. It was observed that γ_S^d (the dispersive surface energy) decreased as the temperature increased. Acid-base constants (K_A and K_D) of pure SBA-15 were found as 0.25 and 0.377, respectively. Since the K_D value is higher than K_A, the surface character was found to be basic. Except for B-SBA-15-10, the surface characters of all samples were found to be alkaline. The addition of boron to the structure did not affect the structure of SBA-15 significantly. It can be said that pure SBA-15 is the most suitable material for adsorption according to the surface areas of samples.

There is no publication in the literature that studies the adsorption thermodynamic parameters of SBA-15 mesoporous materials. Therefore, the data obtained in this study is considered to be important.

Acknowledgements

This work was financially supported by the Scientific Research Foundation at Eskisehir Osmangazi University (Grant number 2013-15049). So, the project team expresses its gratitude for this support. The authors thank Professor Aysegül Aşkın for her experience.

References

[1] Zhao D. Triblock copolymer syntheses of mesoporous silica with periodic 50 to 300 angstrom pores. Science 1998;279:548–52. https://doi.org/10.1126/science.279.5350.548. 80-.
[2] Zhao D, Huo Q, Feng J, Chmelka BF, Stucky GD. Nonionic triblock and star diblock copolymer and oligomeric surfactant syntheses of highly ordered, hydrothermally stable, mesoporous silica structures. J Am Chem Soc 1998;120:6024–36. https://doi.org/10.1021/ja974025i.
[3] Taguchi A, Schüth F. Ordered mesoporous materials in catalysis. Microporous Mesoporous Mater 2005;77:1–45. https://doi.org/10.1016/j.micromeso.2004.06.030.
[4] Huirache-Acuña R, Nava R, Peza-Ledesma C, Lara-Romero J, Alonso-Núez G, Pawelec B, et al. SBA-15 mesoporous silica as catalytic support for hydrodesulfurization catalysts—review. Materials 2013;6:4139–67. https://doi.org/10.3390/ma6094139.
[5] Eswaramoorthi I, Dalai AK. Synthesis, characterisation and catalytic performance of boron substituted SBA-15 molecular sieves. Microporous Mesoporous Mater 2006;93:1–11. https://doi.org/10.1016/j.micromeso.2006.01.018.
[6] Zhang L, Zhao Y, Dai H, He H, Au CT. A comparative investigation on the properties of Cr-SBA-15 and CrOx/SBA-15. Catal Today 2008;131:42–54. https://doi.org/10.1016/j.cattod.2007.10.017.
[7] Van Grieken R, Escola JM, Moreno J, Rodríguez R. Direct synthesis of mesoporous M-SBA-15 (M=Al, Fe, B, Cr) and application to 1-hexene oligomerization. Chem Eng J 2009;155:442–50. https://doi.org/10.1016/j.cej.2009.07.016.
[8] Sun B, Li L, Fei Z, Gu S, Lu P, Ji W. Prehydrolysis approach to direct synthesis of Fe, Al, Cr-incorporated SBA-15 with good hydrothermal stability and enhanced acidity. Microporous Mesoporous Mater 2014;186:14–20. https://doi.org/10.1016/j.micromeso.2013.11.018.
[9] Hami Dindar M, Yaftian MR, Pilehvari M, Rostamnia S. SBA-15 mesoporous materials decorated with organic ligands: use as adsorbents for heavy metal ions. J Iran Chem Soc 2015;12:561–72. https://doi.org/10.1007/s13738-014-0513-8.
[10] Singh S, Nguyen TD, Siang TJ, Phuong PTT, Huy Phuc NH, Truong QD, et al. Boron-doped Ni/SBA-15 catalysts with enhanced coke resistance and catalytic performance for dry reforming of methane. J Energy Inst 2020;93:31–42. https://doi.org/10.1016/j.joei.2019.04.011.
[11] Siang TJ, Pham TLM, Cuong N Van, Phuong PTT, Phuc NHH, Truong QD, et al. Combined steam and CO2 reforming of methane for syngas production over carbon-resistant boron-promoted Ni/SBA-15 catalysts. Microporous Mesoporous Mater 2018;262:122–32. https://doi.org/10.1016/j.micromeso.2017.11.028.
[12] Siang TJ, Bach LG, Singh S, Truong QD, Ho VTT, Huy Phuc NH, et al. Methane bi-reforming over boron-doped Ni/SBA-15 catalyst: longevity evaluation. Int J Hydrogen Energy 2019;44:20839–50. https://doi.org/10.1016/j.ijhydene.2018.06.123.
[13] Wang N, Chu W, Zhang T, Zhao XS. Synthesis, characterization and catalytic performances of Ce-SBA-15 supported nickel catalysts for methane dry reforming to hydrogen and syngas. Int J Hydrogen Energy 2012;37:19–30. https://doi.org/10.1016/j.ijhydene.2011.03.138.
[14] Schuster JM, Schvezov CE, Rosenberger MR. Construction and calibration of a goniometer to measure contact angles and calculate the surface free energy in solids with uncertainty analysis. Int J Adhesion Adhes 2018;87:205–15. https://doi.org/10.1016/j.ijadhadh.2018.10.012.
[15] Rückriem M, Inayat A, Enke D, Gläser R, Einicke WD, Rockmann R. Inverse gas chromatography for determining the dispersive surface energy of porous silica. Colloids Surfaces A Physicochem Eng Asp 2010;357:21–6. https://doi.org/10.1016/j.colsurfa.2009.12.001.
[16] Aşkin A, Bilgiç C. Thermodynamics of adsorption of hydrocarbons on molecular sieves NaY and CaY by inverse gas chromatography. Chem Eng J 2005;112:159–65. https://doi.org/10.1016/j.cej.2005.04.017.
[17] Newell HE, Buckton G. Inverse gas chromatography: investigating whether the technique preferentially probes high energy sites for mixtures of crystalline and amorphous lactose. Pharm Res (N Y) 2004;21:1440–4. https://doi.org/10.1023/B:PHAM.0000036918.79205.4b.
[18] Khodakarami M, Alagha L, Burnett DJ. Probing surface characteristics of rare earth minerals using contact angle measurements, atomic force microscopy, and inverse gas chromatography. ACS Omega 2019;4:13319–29. https://doi.org/10.1021/acsomega.9b01491.
[19] Hamieh T. Determination of Lewis acid base properties of poly(α-n-alkyl) methacrylates adsorbed on silica by inverse GC. Chromatographia 2011;73:709–19. https://doi.org/10.1007/s10337-011-1925-6.
[20] Yao Z, Wu D, Heng JYY, Lanceros-Méndez S, Hadjittofis E, Su W, et al. Comparative study of surface properties determination of colored pearl-oyster-shell-derived filler using inverse gas chromatography method and contact angle measurements. Int J Adhesion Adhes 2017;78:55–9. https://doi.org/10.1016/j.ijadhadh.2017.06.018.
[21] Thielmann F. Introduction into the characterisation of porous materials by inverse gas chromatography. J Chromatogr A 2004;1037:115–23. https://doi.org/10.1016/j.chroma.2004.03.060.

[22] Rückriem M, Enke D, Hahn T. Inverse gas chromatography (IGC) as a tool for an energetic characterisation of porous materials. Microporous Mesoporous Mater 2015;209:99–104. https://doi.org/10.1016/j.micromeso.2014.08.053.
[23] Lazarević S, Ž Radovanović, Veljović D, Onjia A, Janaćković D, Petrović R. Characterization of sepiolite by inverse gas chromatography at infinite and finite surface coverage. Appl Clay Sci 2009;43:41–8. https://doi.org/10.1016/j.clay.2008.07.013.
[24] Ngeow YW, Williams DR, Chapman AV, Heng JYY. Surface energy mapping of modified silica using IGC technique at finite dilution. ACS Omega 2020;5:10266–75. https://doi.org/10.1021/acsomega.9b03920.
[25] Bilgiç C, Aşkin A. Evaluation of the thermodynamic parameters for the adsorption of some hydrocarbons on alumina and molecular sieves 3A and 5A by inverse gas chromatography. J Chromatogr A 2003;1006:281–6. https://doi.org/10.1016/S0021-9673(03)00429-1.
[26] Schultz J, Lavielle L, Martin C. The role of the interface in carbon fibre-epoxy composites. J Adhes 1987;23:45–60. https://doi.org/10.1080/00218468708080469.
[27] Laub RJ. Physicochemical measurement by gas chromatography. 1979. xix + 632 pages, U.S. $82.50. J High Resolut Chromatogr. In: Conder JR, Young CL, editors3. Chichester): Wiley; 1980. p. 486. https://doi.org/10.1002/jhrc.1240030917. 486.
[28] James AT, Martin AJ. Gas-liquid partition chromatography; the separation and micro-estimation of volatile fatty acids from formic acid to dodecanoic acid. Biochem J 1952;50:679–90. https://doi.org/10.1042/bj0500679.
[29] Thiele H, de Boer von HJ. 431. The dynamical character of adsorption, vol. 65. Oxford University Press; 1953. p. 431. https://doi.org/10.1002/ange.19530651619. 1953. 1. Aufl. X V, 239 S., 45 Abb. gebd. s. 30.—. Angew Chemie.
[30] Vidal A, Papirer E, Jiao WM, Donnet JB. Modification of silica surfaces by grafting of alkyl chains. I-characterization of silica surfaces by inverse gas-solid chromatography at zero surface coverage. Chromatographia 1987;23:121–8.
[31] Rodriguez MA. Application of inverse gas chromatography to the study of the surface properties of slates. Clay Clay Miner 1997;45:670–80. https://doi.org/10.1346/CCMN.1997.0450506.
[32] Chappell PJC, Williams DR. Determination of poly(p-phenylene terephthalamide) fiber surface cleanliness by inverse gas chromatography. J Colloid Interface Sci 1989;128:450–7. https://doi.org/10.1016/0021-9797(89)90360-3.
[33] Milonjić SK. Surface properties of metal ions modified silicas. Colloids Surfaces A Physicochem. Eng. Asp. 1999;149:461–6. https://doi.org/10.1016/S0927-7757(98)00563-9. Elsevier Science Publishers B.V.
[34] Salimi A. Characterization of nano scale adhesion at solid surface of oxidized PP wax/PP blends. Int J Adhesion Adhes 2012;33:61–6. https://doi.org/10.1016/j.ijadhadh.2011.11.004.
[35] Fowkes FM. Role of acid-base interfacial bonding in adhesion. J Adhes Sci Technol 1987;1:7–27. https://doi.org/10.1163/156856187X00049.
[36] Saint Flour C, Papirer E. Gas-solid chromatography: a quick method of estimating surface free energy variations induced by the treatment of short glass fibers. J Colloid Interface Sci 1983;91:69–75. https://doi.org/10.1016/0021-9797(83)90314-4.
[37] Gutmann V. The donor-acceptor approach to molecular interactions | Viktor Gutmann | Springer. first ed. New York: Plenum Press; 1978. Springer US.
[38] Riddle FL, Fowkes FM. Spectral shifts in acid-base chemistry. 1. Van der Waals contributions to acceptor numbers. J Am Chem Soc 1990;112:3259–64. https://doi.org/10.1021/ja00165a001.
[39] Trong On D, Joshi PN, Lemay G, Kaliaguine S. Acidity and structural state of boron in mesoporous boron silicate MCM-41. Stud Surf Sci Catal 1995;97:543–9. https://doi.org/10.1016/S0167-2991(06)81937-3. Elsevier.
[40] Coudurier G, Auroux A, Vedrine JC, Farlee RD, Abrams L, Shannon RD. Properties of boron-substituted ZSM-5 and ZSM-11 zeolites. J Catal 1987;108:1–14. https://doi.org/10.1016/0021-9517(87)90150-3.
[41] Trong On D, Kapoor MP, Bonneviot L, Kaliaguine S, Gabelica Z. Structural state of boron in MFI-titanium boralites and their catalytic properties. J Chem Soc Faraday Trans 1996;92:1031. https://doi.org/10.1039/ft9969201031.
[42] Jahandar Lashaki M, Sayari A. CO2 capture using triamine-grafted SBA-15: the impact of the support pore structure. Chem Eng J 2018;334:1260–9. https://doi.org/10.1016/j.cej.2017.10.103.
[43] Li D, Zeng L, Li X, Wang X, Ma H, Assabumrungrat S, et al. Ceria-promoted Ni/SBA-15 catalysts for ethanol steam reforming with enhanced activity and resistance to deactivation. Appl Catal B Environ 2015;176–177:532–41. https://doi.org/10.1016/j.apcatb.2015.04.020.
[44] Kaydouh MN, El Hassan N, Davidson A, Casale S, El Zakhem H, Massiani P. Highly active and stable Ni/SBA-15 catalysts prepared by a "two solvents" method for dry reforming of methane. Microporous Mesoporous Mater 2016;220:99–109. https://doi.org/10.1016/j.micromeso.2015.08.034.
[45] Wisniewska J, Sobczak I, Ziolek M. Gold based on SBA-15 supports – promising catalysts in base-free glucose oxidation. Chem Eng J 2020:127548. https://doi.org/10.1016/j.cej.2020.127548.
[46] Santos JMRC, Fagelman K, Guthrie J. Characterisation of the surface Lewis acid–base properties of poly(butylene terephthalate) by inverse gas chromatography. J Chromatogr A 2002;969:111–8. https://doi.org/10.1016/S0021-9673(02)00890-7.
[47] Karakehya N, Bilgiç C. Inverse gas chromatographic determination of the surface energy of PMMA and PMMA/organophilic montmorillonite nanocomposites. Surf Interface Anal 2016;48:519–21. https://doi.org/10.1002/sia.5969.
[48] Yao Z, Wu D, Heng JYY, Lanceros-Méndez S, Hadjittofis E, Su W, et al. Comparative study of surface properties determination of colored pearl-oyster-shell-derived filler using inverse gas chromatography method and contact angle measurements. Int J Adhesion Adhes 2017;78:55–9. https://doi.org/10.1016/j.ijadhadh.2017.06.018.
[49] Yao Z, Heng JYY, Lanceros-Méndez S, Pegoretti A, Xia M, Tang J, et al. Surface free energy and mechanical performance of LDPE/CBF composites containing toxic-metal free filler. Int J Adhesion Adhes 2017;77:58–62. https://doi.org/10.1016/j.ijadhadh.2017.04.005.
[50] Schmitt P, Koerper E, Schultz J, Papirer E. Characterization, by inverse gas chromatography, of the surface properties of calcium carbonate before and after treatment with stearic acid. Chromatographia 1988;25:786–90. https://doi.org/10.1007/BF02262085.
[51] Papirer E, Schultz J, Turchi C. Surface properties of a calcium carbonate filler treated with stearic acid. Eur Polym J 1984;20:1155–8. https://doi.org/10.1016/0014-3057(84)90181-2.
[52] Jiao P, Wei Y, Zhang M, Zhang X, Zhang H, Yuan X. Adsorption separation of l-tryptophan based on the hyper-cross-linked resin XDA-200. ACS Omega 2021;6:2255–63. https://doi.org/10.1021/acsomega.0c05574.
[53] Wu C, Lou X, Xu X, Huang A, Zhang M, Ma L. Thermodynamics and kinetics of pretilachlor adsorption on organobentonites for controlled release. ACS Omega 2020;5:4191–9. https://doi.org/10.1021/acsomega.9b04025.
[54] Gereli G, Seki Y, Murat Kuşoğlu I, Yurdakoç K. Equilibrium and kinetics for the sorption of promethazine hydrochloride onto K10 montmorillonite. J Colloid Interface Sci 2006;299:155–62. https://doi.org/10.1016/j.jcis.2006.02.012.
[55] Rauf N, Tahir SS, Kang JH, Chang YS. Equilibrium, thermodynamics and kinetics studies for the removal of alpha and beta endosulfan by adsorption onto bentonite clay. Chem Eng J 2012;192:369–76. https://doi.org/10.1016/j.cej.2012.03.047.